PROCEEDINGS, TOUGH Symposium 2003
Lawrence Berkeley National Laboratory, Berkeley, California, May 12–14, 2003

EVALUATING THE EFFECTIVENESS OF LIQUID DIVERSION AROUND AN UNDERGROUND OPENING WHEN EVAPORATION IS NON-NEGLIGIBLE

Teamrat A. Ghezzehei, Robert Trautz, and Stefan Finsterle

Earth Sciences Division, Lawrence Berkeley National Laboratory
1 Cyclotron Rd., MS 90–1116, Berkeley, CA 94720, United States
E-mail: TAGhezzehei@lbl.gov

ABSTRACT

Interpreting observations of seepage into underground openings is often complicated by evaporative potentials created by the necessity to ventilate the openings. Evaporation removes liquid from the seepage face. By doing so, it reduces both the likelihood of seepage onset and the seepage flux, and thus can enhance the perceived effectiveness of the capillary barrier. We modeled liquid-release tests at the proposed high-level waste repository in Yucca Mountain, using an enhanced version of the EOS9 module of iTOUGH2, which incorporates evaporation as Fickian diffusion. The evaporation boundary layer thickness (BLT) over which diffusion occurs was estimated using free-water evaporation experiments conducted at Yucca Mountain under known relative humidity, temperature, and ventilation conditions. The BLT, which represents the thickness of the laminar flow regime, is inversely related to the ambient airflow velocity. At Yucca Mountain, the estimated values of BLT were 5–7 mm for open underground tunnels and 20 mm for closed niches. Compared to previous models that neglected the effect of evaporation, this new approach shows significant improvement in capturing seepage fluctuations into the open tunnels. This study provides more confidence in the use of the calibrated seepage model for simulations of seepage under different ventilation conditions.

INTRODUCTION

Continuum models of flow in unsaturated fractured rock and the associated seepage into underground openings can be calibrated against field liquid release tests to provide *effective*, *model-related*, and *process-specific* properties of the porous medium (Finsterle, 2000). Previous calibration exercises ignored the contribution of evaporation in reducing seepage, although the calibration data was obtained from field tests conducted in ventilated cavities (e.g., Finsterle and Trautz, 2001; Trautz and Wang, 2001). Recently, Trautz and Wang (2002) accounted for the role of evaporation in reducing seepage by considering an empirical relationship between relative humidity and free-water evaporation measured in an environment similar to where the seepage tests were conducted. However, the empirical relationship is applicable only to free-water evaporation under similar conditions. Ahlers et al. (2003) used an alternative semi-physical approach to modeling evaporation from a porous medium. They modeled evaporation as an isothermal vapor-diffusion process that accounts for the relative humidity and temperature of the air. Ahlers et al. (2003) updated the EOS9 module of iTOUGH2 to include a special evaporation connection that implements the diffusion equation. The evaporation model assumes evaporation as a vapor diffusion process occurring across a finite boundary layer. The vapor concentration at the rock face was related to the wetness of the rock, and the vapor concentration of the bulk air is related to the humidity.

The objectives of this paper are: (1) to provide a calibrated estimate of the boundary layer thickness and (2) to assess the role of evaporation in a seepage calibration model.

EVAPORATION BOUNDARY LAYER

Theory

Evaporation from a free liquid surface involves vapor diffusion by virtue of a vapor-concentration gradient adjacent to the liquid surface, as illustrated by the solid-line curve in Figure 1. The diffusion equation that governs the mass flux of vapor J_V [kg m^{-2} s^{-1}] is given by

$$J_V = -D\frac{dC}{dz}, \qquad (1)$$

where C [kg m^{-3}] is vapor density, D [m^2 s^{-1}] is the vapor diffusion coefficient, and z [m] is physical distance. The air immediately in contact with the liquid water is saturated with vapor, and the saturated vapor concentration is related to the saturated partial pressure of vapor by

$$C^\circ = \frac{p_S(T^\circ)\cdot M_w}{R\cdot T^\circ}, \qquad (2)$$

where M_w [0.01802 kg mol^{-1}] is the molecular weight of water, R [8.314 J K^{-1} mol^{-1}] is the universal gas constant, and $p_S(T)$ [Pa] is the saturated partial pressure of vapor for liquid surface temperature of $T = T^\circ$ [K]. Similarly, the vapor concentration in the bulk air is related to relative humidity of the air h [dimensionless] and air temperature $T = T^\infty$ by

$$C^{\infty} = \frac{p_S(T^{\infty}) \cdot M_w}{R \cdot T^{\infty}} \cdot h \,. \qquad (3)$$

As the vapor moves away from the liquid surface by diffusion, it is continuously replenished by evaporation of additional liquid water – a heat consuming process. The natural tendency of the diffusion process is to reach equilibrium by attempting to elevate the bulk-air humidity to saturation.

To facilitate estimation of evaporation as a vapor-diffusion process, we introduce the following assumptions:

1. The relative humidity (h) of the bulk-air is fixed externally, hence, C^{∞} is constant
2. The heat consumed by vaporization is supplied externally, so that the temperature at the liquid surface ($T°$) is maintained; hence, $C°$ is constant.
3. Isothermal conditions exist. The temperature of the air immediately in contact with the water surface is equal to the air temperature removed from the surface, $T^{\infty} = T° = T$

For evaporation from a large area of liquid (negligible edge effects), consideration of mass conservation implies that the vapor mass flux (J_V) is constant at all distances within the boundary layer. Then, Eq. (1) and the above assumptions imply that the vapor concentration gradient is also constant, leading to an approximate expression of vapor diffusion:

$$J_V \approx -\frac{D \cdot p_S(T) \cdot M_w}{R \cdot T} \frac{(1-h)}{\delta} \,, \qquad (4)$$

where δ [m] is an effective boundary-layer thickness, within which the vapor concentration is assumed to linearly decrease from full saturation to a value dictated by the air humidity (dashed curve).

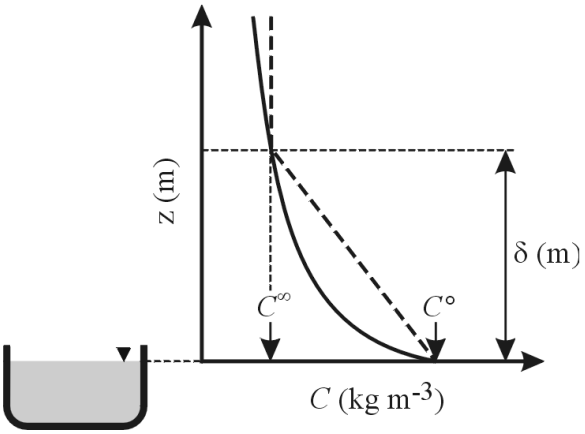

Figure 1. Schematic description of vapor concentration gradient above a free water surface

The thickness of the boundary layer is closely related to the airflow velocity profile above the liquid. For laminar airflow, the boundary-layer thickness is inversely related to the bulk airflow velocity (Rohsenow and Choi, 1961). Thus, the approximate evaporation rate of Eq. (4) accounts for the most important evaporation-related environmental factors: (1) temperature, (2) humidity, and (3) ventilation (airflow velocity) conditions.

Estimation of Boundary Layer Thickness (δ)

In the following, we show estimation of the boundary layer thickness (•) by calibration of the evaporation rate given by Eq. (4) against measured data.

At the Exploratory Studies Facility (ESF) of Yucca Mountain, relative humidity and temperature were measured at 11 locations inside a 15-m long experimental niche (Niche 1620) closed by a bulkhead. (A *niche* is a short excavation constructed off the main ESF tunnel for field experiments.) Similar measurements were conducted at one location outside the closed niche. Simultaneously, free-water evaporation rates inside and outside the niche were automatically recorded.

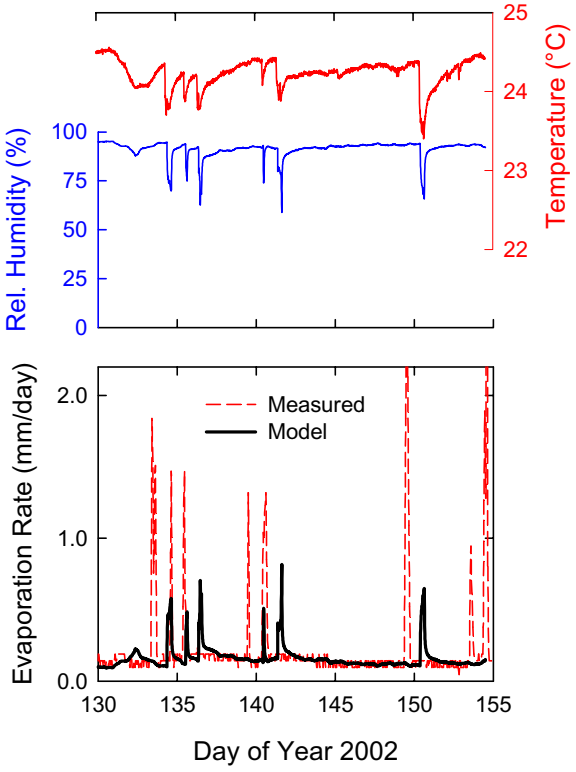

Figure 2. Relative humidity, temperature and evaporation rate data collected inside Niche 1620

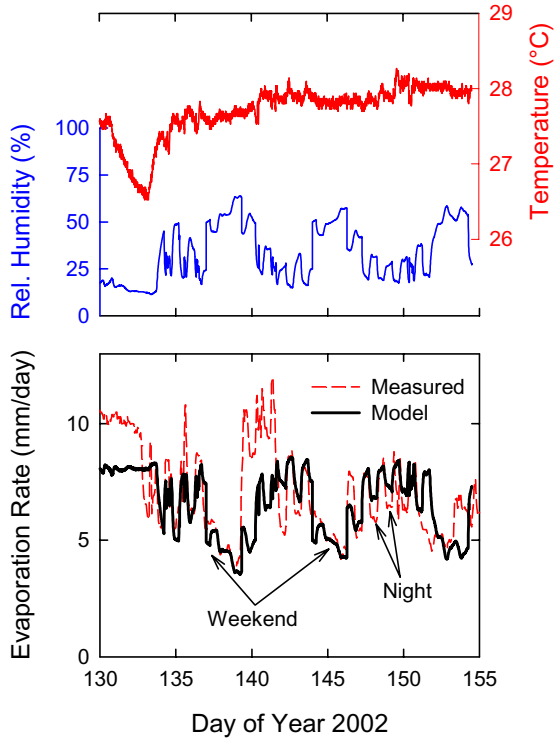

Figure 3. Relative humidity, temperature and evaporation rate data collected outside Niche 1620

The available evaporation data were grouped into three classes based on airflow velocity: (1) inside Niche 1620 without ventilation; (2) outside Niche 1620 with active ventilation; and (3) outside Niche 1620 without active ventilation, the regime usually encountered during nights and weekends. In Figure 2 and Figure 3, the measured relative humidity and temperature, as well as measured and fitted evaporation rates, are plotted for inside and outside Niche 1620, respectively. The best-fit estimates of the boundary layer thickness are listed in Table 1. Inside the niche, the air is expected to be relatively calm because it is isolated from the main tunnel of the ESF. As a result, the thickest boundary layer (20 mm) develops there. Figure 3 shows that the relative humidity outside Niche 1620 increases at nights and during weekends when active tunnel ventilation is turned off. However, this increase in relative humidity is not sufficient to explain the observed decrease in evaporation. Therefore, as shown in Table 1, reduced air ventilation during nights and weekends is also accompanied by an increase in the thickness of the boundary layer. These results confirm the applicability of Eq. (4) to describe the roles of humidity, temperature, and ventilation on evaporation rate. Note that the isothermal approximation of evaporation is incapable of predicting evaporation correctly in instances that cause abrupt temperature changes.

Table 1 Boundary-layer thickness estimates

Location of Experiment	•(mm)
Inside Niche	20.0
Outside Niche, ventilation off	7.5
Outside Niche, ventilation on	5.0

DRIFT-SCALE SEEPAGE MODELING

Water flow through the fractured welded tuff and seepage into openings at Yucca Mountain occurs predominantly through the fracture network. Finsterle (2000) showed that this process can be simulated using a heterogeneous fracture continuum model, provided that the model is calibrated against seepage-relevant data. In the following subsections we present the calibration of a seepage model that accounts for possible evaporation from the ceiling and sidewalls of subsurface openings.

Field Tests

The seepage data used in calibrating the model were obtained from two different liquid-release tests conducted in the lower lithophysal zone of the Topopah Spring welded tuff unit of Yucca Mountain. The general design of both tests is similar. Liquid is released at a controlled rate into boreholes drilled above a drift or niche. The part of the released liquid that drips into the excavation is collected by a capture system connected to automated gauging devices. During the tests relative humidity and temperature of the air in the excavation are monitored.

ECRB Test

Liquid-release tests were conducted in a circular drift of 5 m diameter excavated off the ESF for Enhanced Characterization of the Repository Block (ECRB). Liquid-release boreholes of approximately 20 m length were drilled above the ECRB parallel to the axis of the ECRB. The data discussed here were obtained from a particular borehole SYBT-ECRB-LA#2, which is upward-inclined at a nominal 15° from the drift axis. Packers were set to isolate three 1.8 m long injection zones named zone 1, zone 2, and zone 3. The data used herein were obtained from zone 3, in which the liquid-release point is approximately 2.5 m above the crown of the drift. Although the drifts were actively ventilated, air circulation in the test zone was partially reduced by curtains installed on the two sides of the capture system.

Niche Test

The data used here were obtained from tests conducted in Niche 1620, which is approximately 15 m in length and 4 m in width. The liquid release bore-

hole (borehole #4) was located approximately 1.25 m above the crown of the niche and was 1 m off the niche axis. The entrance to the niche was closed by a bulkhead, which significantly reduced air circulation between the niche and the ECRB.

Numerical Model

The seepage model is conceptualized as a three-dimensional, heterogeneous continuum model. The continuum mainly represents the dense fracture network that dominates the seepage process. Three-dimensional numerical meshes representing the ECRB drift (Figure 4) and Niche 1620 (Figure 5) were generated with grid sizes of 0.1 m × 0.3 m × 0.1 m and 0.1 m × 0.1 m × 0.1 m, respectively. Heterogeneous permeability fields were mapped onto the numerical meshes using geostatistical parameters obtained from measured permeability data. For symmetry reasons, the ECRB mesh considers only half of the circular cylindrical drift. In contrast, the full asymmetric niche was modeled. The roughness of the niche ceiling was taken into account in the numerical mesh.

No-flow boundary conditions are specified at the left, right, front, and back sides of the model. A free-drainage boundary condition is applied at the bottom to prevent an unphysical capillary boundary effect. All elements representing large openings (i.e., borehole intervals, drift sections, or niches) are assigned a zero capillary pressure independent of saturation. The evaporation elements are set at a capillary pressure equivalent to the prevailing relative humidity h according to Kelvin's equation:

$$p_c = -\frac{RT}{M_w}\rho_w \ln(h)\,. \qquad (5)$$

where ρ_w is density of water. Evaporation from the elements at the drift and niche boundary into the drift element is calculated as described by Ahlers et al. (2003). For the ECRB test, the relative humidity of the evaporation element was changed periodically according to values measured during the liquid release test. The relative humidity of the niche test was fixed at a value of 85 %, which was an average of the almost constant condition observed in the niche during the test. Liquid water is allowed to enter (seep), but prevented from exiting the drift or niche. A constant flux (approximately 13.6 mm/yr) boundary condition was applied at the top of the model to represent background percolation. For the simulation of liquid-release tests, release rates and test durations are determined for each event and applied to the elements representing the injection interval.

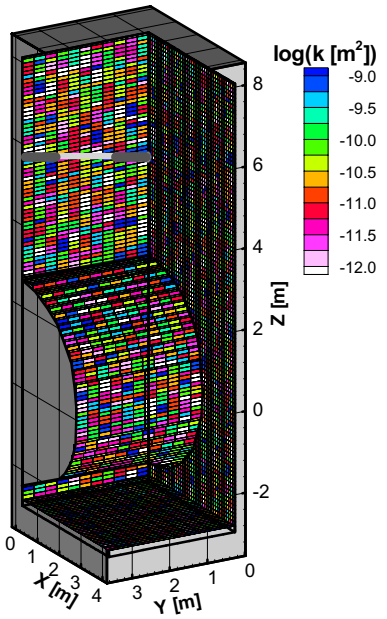

Figure 4. Numerical mesh of the ECRB drift.

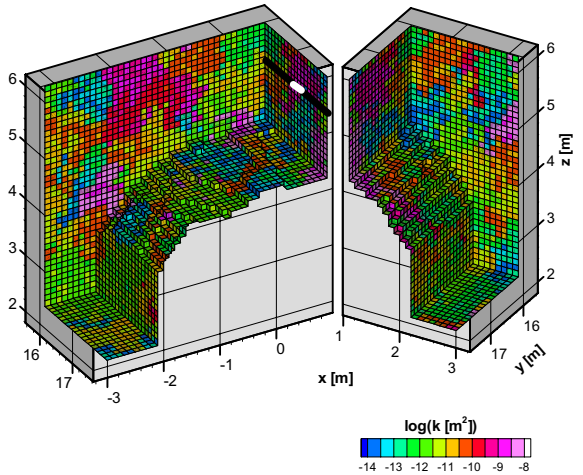

Figure 5. Numerical mesh of Niche 1620.

The relative permeability and capillary pressure of the elements representing the fracture continuum were related to liquid saturation by the van Genuchten relations (van Genuchten, 1980). The four main parameters that describe flow properties of the fractured porous medium are: (1) the van Genuchten capillary-strength parameter $1/\alpha$ [Pa]; (2) n [dimensionless], which is related to the van Genuchten parameter m by $n = 1/(1-m)$; (3) the reference permeability of the heterogeneous permeability field k [m^2]; and (4) the effective porosity ϕ [dimensionless]. A sensitivity analysis determined that seepage rate is only slightly affected by porosity ϕ and parameter m. Therefore, these parameters were assigned fixed values of 1 % and 0.611, respectively, derived from the mountain scale studies. The refer-

ence permeability was assigned the mean of measured air permeability in the respective test regions. The capillary-strength parameter is estimated as an effective, seepage-relevant, model-related parameter through automatic calibration of the seepage calibration model against seepage-rate data from liquid-release tests using iTOUGH2 V5.0.

Results and Discussion

ECRB Test

The long-term liquid-release tests presented here were conducted for about 35 days at an approximate release rate of 40 mL/min. The relative humidity in the testing area (partly protected from air circulation by curtains installed at the two ends of the seepage capture system) varied between 30 and 90 %. The liquid-release rate, seepage rate and relative humidity of the testing area are shown in Figure 6. Fluctuations in seepage rate can be correlated to the drastic changes in relative humidity, which drives evaporation. The model captures this evaporation effect reasonably well, tracking increases in measured seepage rates as relative humidity increases and vice versa. The reported seepage rate is a mean of 21 independent inversions with different realizations of the heterogeneous permeability field. The mean and standard deviation of the estimated capillary strength parameter $1/\alpha$ were 557 and 56 Pa, respectively.

Niche Test

In Niche 1620, borehole #4, a liquid-release test was conducted for 14 days at a fairly constant release rate of approximately 10 mL/min. The observed relative humidity was on average 85 % with only slight fluctuations. The liquid-release rate and seepage rate are shown in Figure 7. As shown in Figure 7, the calculated seepage rate matches the late-time observed seepage rate very well. The reported seepage rate is a mean of 30 independent inversions with different realizations of the heterogeneous permeability field. The mean and standard deviation of the estimated capillary-strength parameter $1/\alpha$ were 671 and 223 Pa, respectively.

In both tests, the model does not describe the transient early stages of the test well because the continuum model does not account for the discreteness of fractures responsible for transient flow. Moreover, a storage effect caused by flow into lithophysal cavities, matrix imbibition, and the drying of the formation (which may not be properly accounted for by the effective porosity) could contribute to this poor early-time prediction.

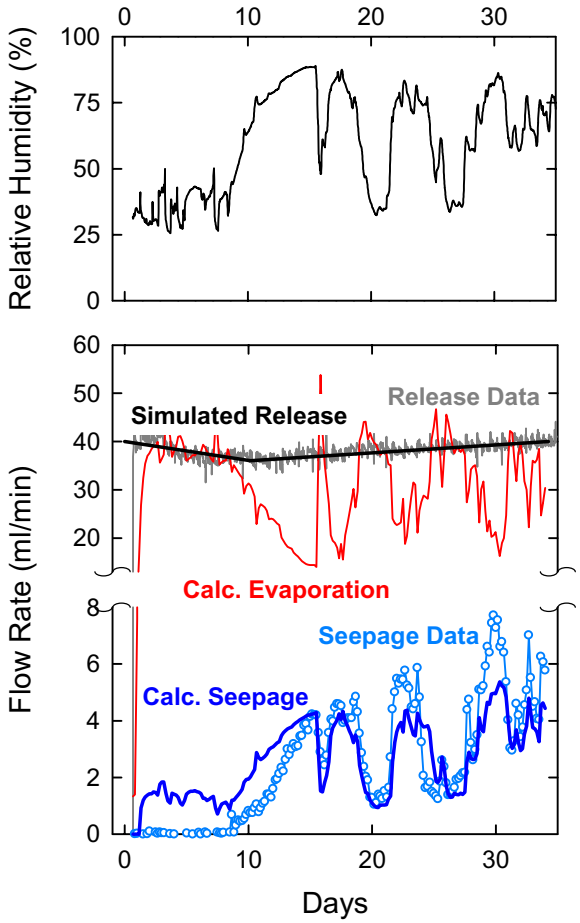

Figure 6. Calibration of seepage-rate data from liquid-release tests conducted in zone 3 of borehole SYBT-ECRB-LA#2

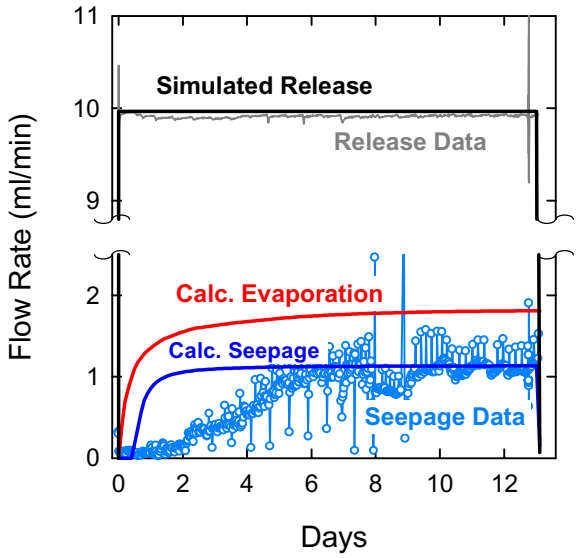

Figure 7. Calibration of seepage-rate data from liquid-release tests conducted in borehole #4 of Niche 1620.

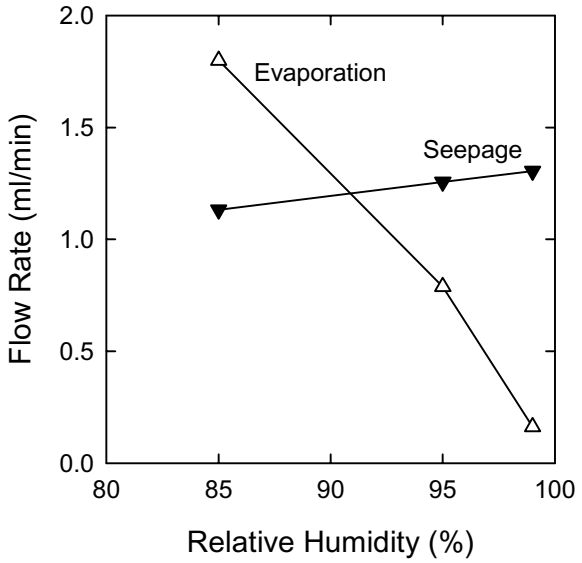

Figure 8. Calculation of seepage and evaporation rates on Day 10 of the liquid-release tests conducted in borehole #4 of Niche 1620.

To test the effect of high relative humidity ($\geq$ 85 %) on seepage, we repeated the simulations with relative humidity values of 95 and 99 %. The resulting seepage and evaporation rates on Day 10 are plotted in Figure 8. Figure 8 shows that evaporation from the entire niche wall surface is relatively high and comparable to the amount of seepage. Evaporation decreases almost linearly as relative humidity increases, as expected. Nevertheless, the impact of evaporation on the calculated seepage rate is small for these high relative humidity values.

CONCLUSIONS

In this paper, we (1) estimated the evaporative boundary-layer thickness by calibrating a semi-physical evaporation model, which considers isothermal vapor diffusion; (2) calibrated a heterogeneous fracture-continuum model against seepage-rate data; and (3) tested the effect of evaporation on seepage predictions.

The simplified vapor-diffusion approach of modeling evaporation was found to be effective in capturing the roles of the important environmental conditions that affect evaporation – namely, relative humidity, temperature, and ventilation. Calibrated thicknesses of the evaporation boundary layer were obtained for three ventilation conditions representing the conditions at the liquid-release test sites at Yucca Mountain.

We found that evaporation reduces seepage significantly in tests conducted under ventilated conditions. Therefore, it is important to account for evaporation effects when calibrating a seepage process model against liquid-release-test data collected under ventilated conditions. In contrast, the impact of evaporation on seepage rate was minimal in closed-off niches, where relative humidity values were generally high. Thus, when using data obtained from closed-off and/or artificially humidified niches, ignoring the effect of evaporation is expected to introduce little error in the estimation of seepage-relevant parameters.

ACKNOWLEDGMENT

We thank Sonia Salah, Yingqi Zhang and Daniel Hawkes for their thorough review. This work was supported by the Director, Office of Civilian Radioactive Waste Management, U.S. Department of Energy, through Memorandum Purchase Order EA9013MC5X between Bechtel SAIC Company, LLC and the Ernest Orlando Lawrence Berkeley National Laboratory (Berkeley Lab). The support is provided to Berkeley Lab through the U.S. Department of Energy Contract No. DE-AC03-76SF00098.

REFERENCES

Ahlers, C.F., T.A. Ghezzehei, and S. Finsterle, Development and testing of a method for efficient simulation of evaporation from a seepage face, in *TOUGH Symposium 2003*, Lawrence Berkeley National Laboratory, Berkeley, California, 2003.

Finsterle, S., Using the continuum approach to model unsaturated flow in fractured rock, *Water Resour. Res*, 36 (8), 2055-2066, 2000.

Finsterle, S., and R.C. Trautz, Numerical modeling of seepage into underground openings, *Mining Eng.*, 53 (9), 52-56, 2001.

Rohsenow, W.M., and H. Choi, *Heat, mass and momentum transfer*, Prentice-Hall Inc., Englewood Cliffs, New Jersey, 1961.

Trautz, R.C., and J.S.Y. Wang, Evaluation of seepage into an underground opening using small- scale field experiments, Yucca Mountain, Nevada, *Mining Eng.*, 53 (12), 41-44, 2001.

Trautz, R.C., and J.S.Y. Wang, Seepage into an underground opening constructed in unsaturated fractured rock under evaporative conditions - art. No. 1188, *Water Resour. Res*, 38 (10), 1188, 2002.

van Genuchten, M.T., A closed-form equation for predicting the hydraulic conductivity of unsaturated soils, *Soil Sci. Soc. Am. J.*, 44 (5), 892-898, 1980.